Supporting Information

3D silver nanoparticles with Multilayer graphene oxide as a Spacer for Surface Enhanced Raman Spectroscopy Analysis

Zhen Li,[a] *Shouzhen Jiang,*[a] *Yanyan Huo,**[a] *Tingyin Ning,*[a] *Aihua Liu,*[a] *Chao Zhang,*[a] *Yuan He,*[a] *Minghong Wang,*[a] *Chonghui Li,*[a] *Baoyuan Man**[a]

School of Physics and Electronics, Shandong Normal University, Jinan 250014, China.

E-mail: 514080202@qq.com, byman@sdnu.edu.cn

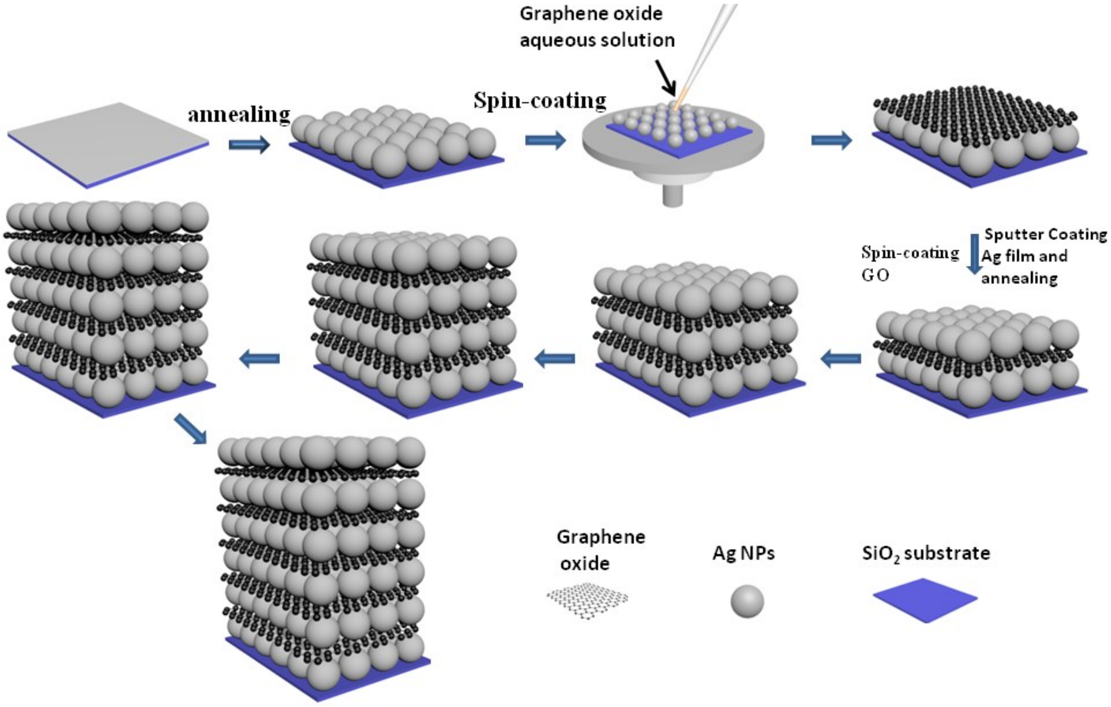

Fig. S1 Schematic illustration of the fabrication of different layers of Ag NPs using mutilayer GO as spacer.

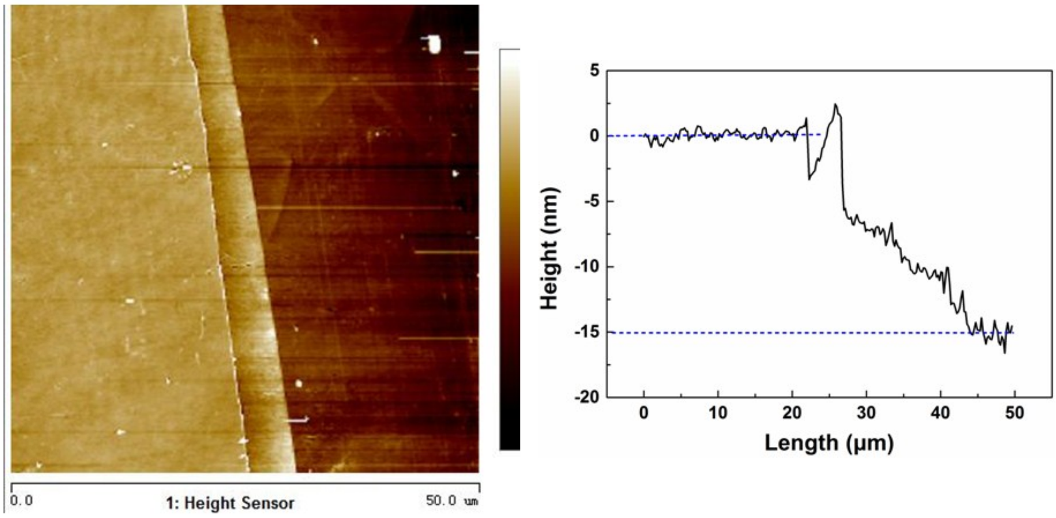

Fig. S2 AFM image of Ag film and its corresponding height profile.

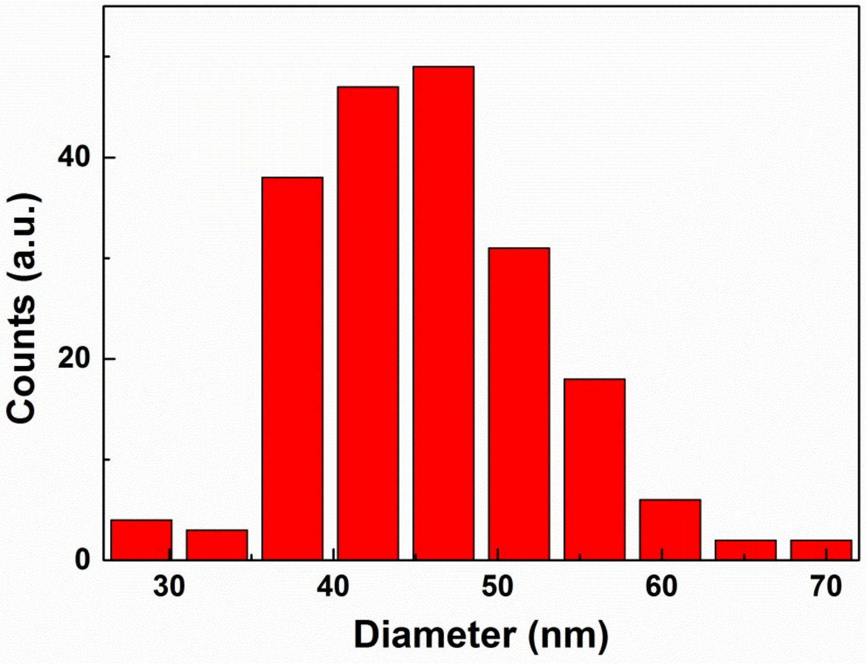

Fig. S3 The statistical histograms of the size of Ag NPs.

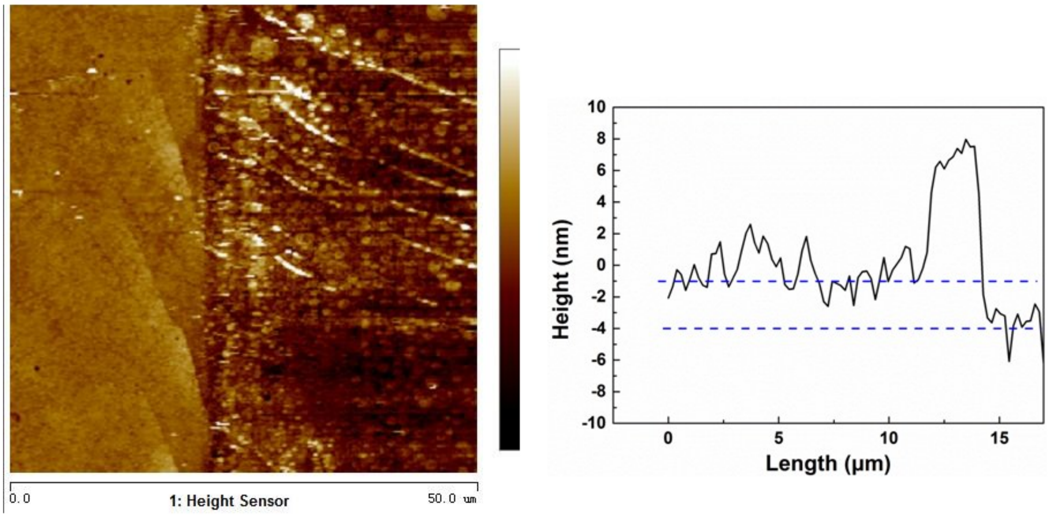

Fig. S4 AFM image of mutilayer GO and its corresponding height profile.

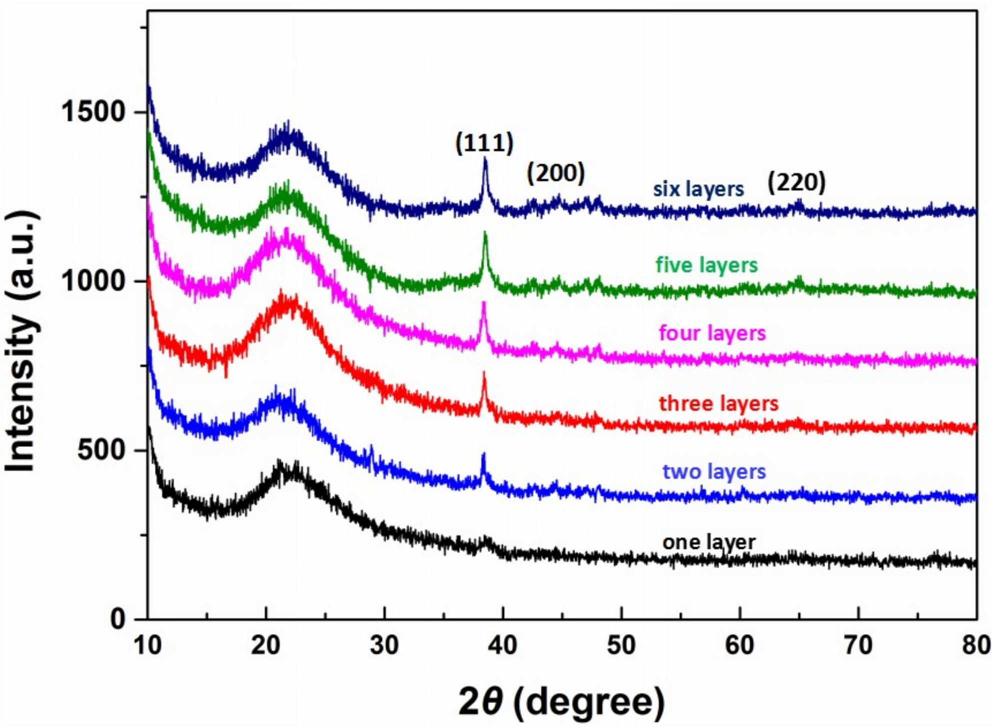

Fig. S5 XRD patterns of the 3D Ag NPs nanostructures with different Ag NPs layers using GO as spacer.

Detailed explanation for the fact that very few probe molecules can penetrate into the 3D structure

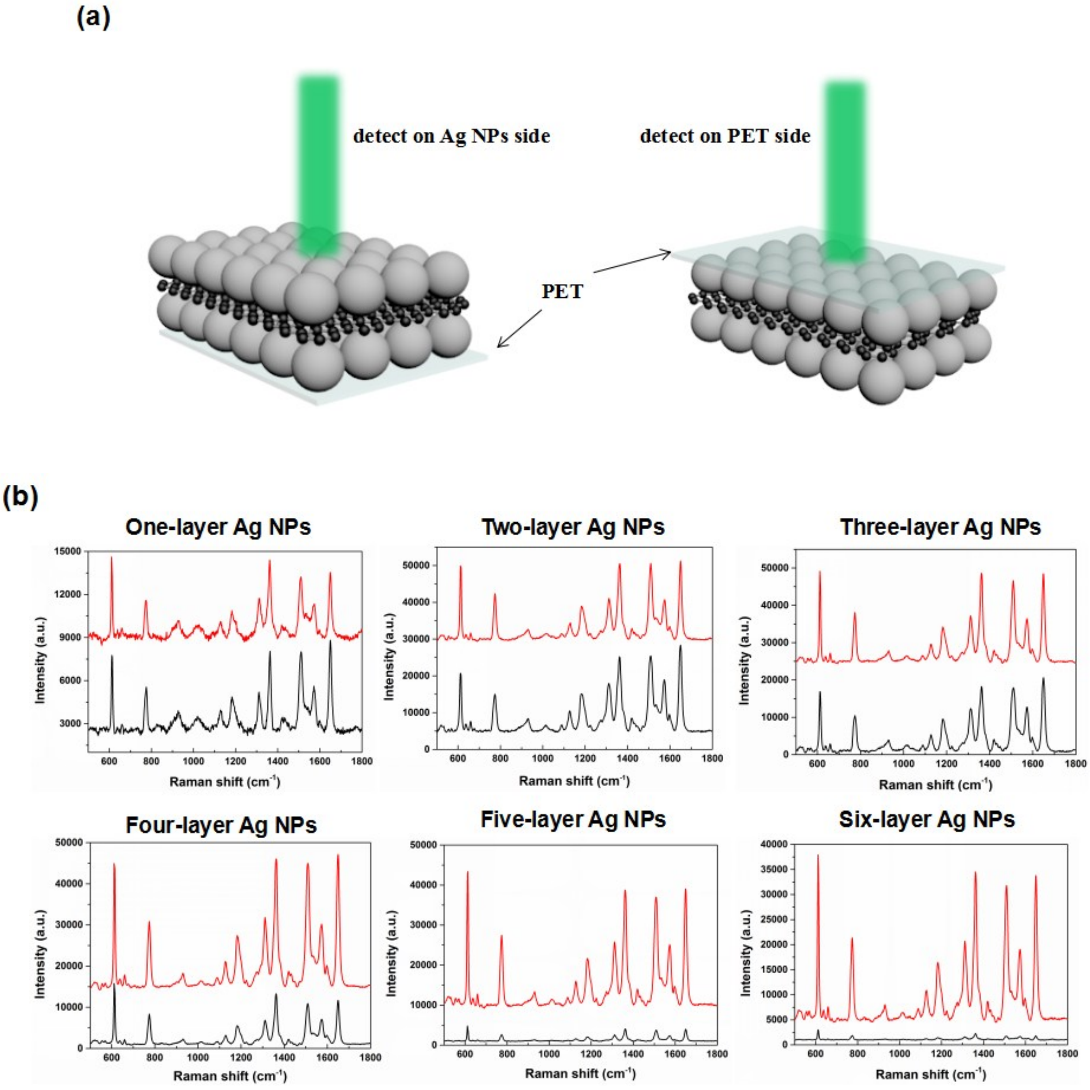

Fig. S6 (a) Schematic illustration of the two detection way for the 3D structure. (b) SERS signal of R6G detected on PET side (black line) and on Ag NPs side (red line) was adopted for study.

To investigate whether the analytes could penetrate the GO film, we fabricate the 3D structure with different Ag NPs layers using GO as spacer on the ultra-thin polyethylene terephthalate (PET) which is a kind of stable polymer with high transparency. Fig. S6a schematically exhibits the two SERS detection way for the 3D structure on PET. 2 μL R6G (10^{-7} M) was firstly deposited on the Ag NPs side. SERS signal of R6G detected on PET side (black line) and on Ag NPs side (red line) are shown in Fig. S6b. In the one-layer and two-layer Ag NPs structure, we found that the R6G signals observed from the Ag NPs side are almost identical with that obtained from the PET side which indicates that the PET is almost no influence for the SERS detection. However, for the SERS signal obtained from the three-layer and four-layer Ag NPs structure, we note that the intensity of the R6G signal obtained from the Ag NPs side is stronger than that obtained from the PET side. The result can be explained by these factors: first, for the PET side detection, the Raman scattered signal of R6G should penetrate the three or four layers Ag NPs to be collected by the Raman detectors and there should exists inevitable optical losses. The Ag NPs side detection is more easy to obtain the Raman scattered signal of R6G. Second, few probe molecules can penetrate into the 3D structure.

The thickness of the four-layer Ag NPs in this 3D structure should be the maximum penetration depth that the incident laser can penetrate, which has been proved in main article. However, for the five-layer and six-layer Ag NPs structure, the R6G signals can be still observed on the PET side, which demonstrates that the probe molecules can indeed penetrate into the 3D structure. Besides, we can observe that the SERS signals of R6G obtained from the Ag NPs side are significantly stronger than that obtained from the PET side. It is indicated that only very few probe molecules can penetrate into the 3D structure for the obstruction of the thick GO films. Thus, the SERS performance of the 3D nanostructures can be mainly attributed to the topmost hot spots. The electromagnetic field intensity of the topmost hot spots is related closely to the number of Ag NPs layers which is investigated both in experiments and theoretical modeling in the main article.

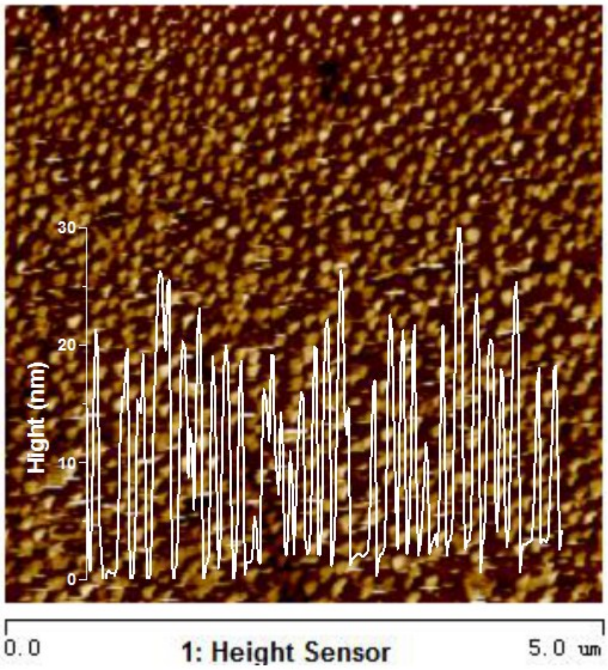

Fig. S7 the AFM image of the Ag NPs and its corresponding height profile.

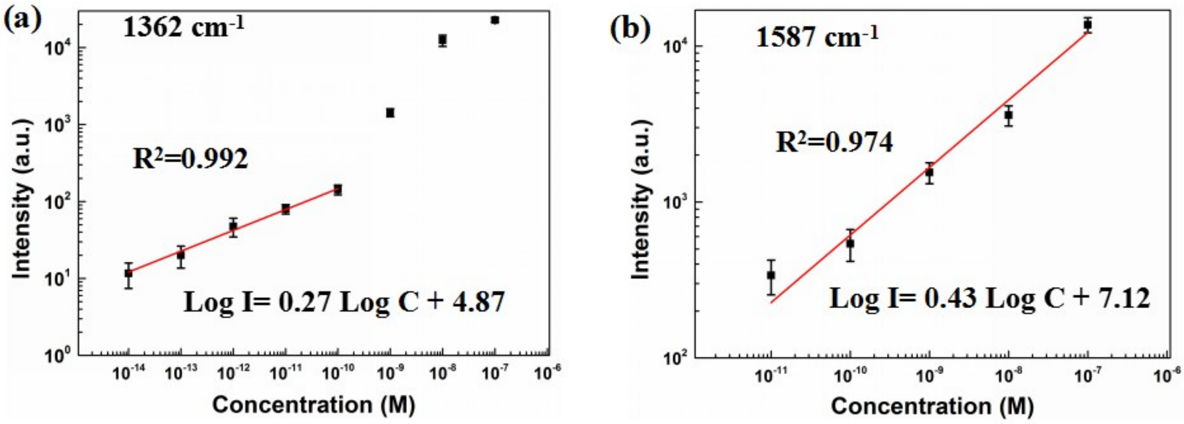

Fig. S8 SERS intensity at 1362 cm^{-1} (a) as a function of R6G molecular concentration and 1587 cm^{-1} (b) as a function of CV molecular concentration. Error bars indicate standard deviations from at least 30 spectra.

Detailed calculative process of the enhancement factor

Rhodamine 6G (R6G) and Crystal violet (CV) were dissolved in water to obtain the solution from 10^{-2} to 10^{-15} M and from 10^{-2} to 10^{-12} M, respectively. When the concentrations of R6G are lower than 10^{-11} M, we can only obtain the SERS signal of R6G from the edge of the final evaporation imprint. Thus, to guarantee the scientific nature of the results, the 10^{-11} M R6G solution was chosen as the limit concentration for calculation of the enhancement factor. Similarly, the 10^{-10} M CV was chosen as the limit concentration for calculation of the enhancement factor. 2 μL R6G with the concentration 10^{-2} and 10^{-11} M were dropped separately on the SiO_2 substrate and fabricated SERS substrates. 2 μL CV with the concentration 10^{-2} and 10^{-10} M were also dropped separately on the SiO_2 substrate and fabricated SERS substrates. Before carrying out the Raman detection, the samples were all totally dried. The estimated maximum diameter of the final evaporation imprint on SiO_2 substrate were around 2.5 mm for R6G (10^{-2} M) and CV (10^{-2} M). And the estimated maximum diameter of the final evaporation imprint were around 2 mm for R6G (10^{-11}M) and CV (10^{-10} M) for the hydrophobic property of the fabricated substrate. Thus, the average areal density (AD) of the R6G and CV can be estimated by the following equation: $AD = CVN / S$, where V, C, N and S represent the volume of the analytes solution dropped, the concentration of analytes solution, Avogadro constant and the area of the analytes molecules covered, respectively.

With the R6G concentration of 10^{-11} M, the AD is around 3.83 molecules/μm^2.

With the CV concentration of 10^{-10} M, the AD is around 38.3 molecules/μm^2.

With the R6G and CV concentration of 10^{-2} M, the AD on SiO_2 is around $2.45*10^9$ molecules/μm^2.

The enhancement factor was estimated by the following equation: $\mathrm{EF} = (I_{\mathrm{SERS}} \times N_{SiO_2})/(I_{SiO_2} \times N_{SERS})$, where I_{SERS}, I_{SiO_2}, N_{SiO_2} and N_{SERS} represent the intensity of SERS signal, Raman signal intensity obtained from SiO_2, the number of analytes molecules within laser spot on SiO_2 substrate and the number of molecules within laser spot on SERS substrate, respectively. The Raman spectrometer was all used under the condition (0.3 mW laser power, × 50 objective lens, 1 μm laser spot). The Raman signal intensity of R6G (10^{-11} M) and CV (10^{-10} M) obtained from 3D SERS substrate, R6G (10^{-2} M) and CV (10^{-2} M) collected from SiO_2 substrate are shown in Fig. 5c and d. Thus, the average EF of the 3D SERS substrate for R6G and CV can be obtained.

Table 1 Comparison of our work with other 3D SERS substrates reported.

Structure	Calculation method	EF	Reference
GO/AgNPs/pyramidal silicon	AEF=(I_{SERS}×N_{Raman}) /(I_{Raman}×N_{SERS}) 10^{-3} M R6G solution on pyramidal silicon and 10^{-11} M on the structure	1.27 × 10^{8}	37
CuNPs/graphene/Cu film	EF = (I_{SERS} /I_{bulk}) × (N_{bulk} /N_{SERS}) 0.5 nm CuPc on the structure and 100 nm CuPc on the silicon substrate	1.9 × 10^{7}	23
3D cross-point plasmonic nanostructures	AEF=(I_{SERS}×N_{film}) /(I_{Normal}×N_{SERS}) 10^{-3} M R6G and 10^{-11}M on the structure	4.1 × 10^{7}	33
AuNPs/Multilayer Graphene/ AuNPs	EF = (I_{SERS} /I_{REF}) × (N_{REF} /N_{SERS}) 10^{-2} M BCB on a glass substrate and 10^{-6}M on the structure	2.89 × 10^{5}	25
Multiple Ag NPs	EF = (I_{SERS} /I_{bulk}) × (N_{bulk} /N_{SERS}) 10^{-9} M R6G on the structure and solid R6G	1.5 ×10^{7}	34
Silver nanoislands on silica spheres	EF = ($I_{platform}$ /$I_{platform}$) × ($N_{reference}$ /$N_{reference}$), 10^{-3} M R6G on the silicon wafer and 10^{-11}M on the structure	3.76 × 10^{7}	38
Multilayer Ag NPs using GO as spacer	AEF=(I_{SERS}×N_{SiO2}) /(I_{SiO2}×N_{SERS}) 10^{-2} M R6G on SiO_2 and 10^{-11} on the structure	7×10^{8}	Current work

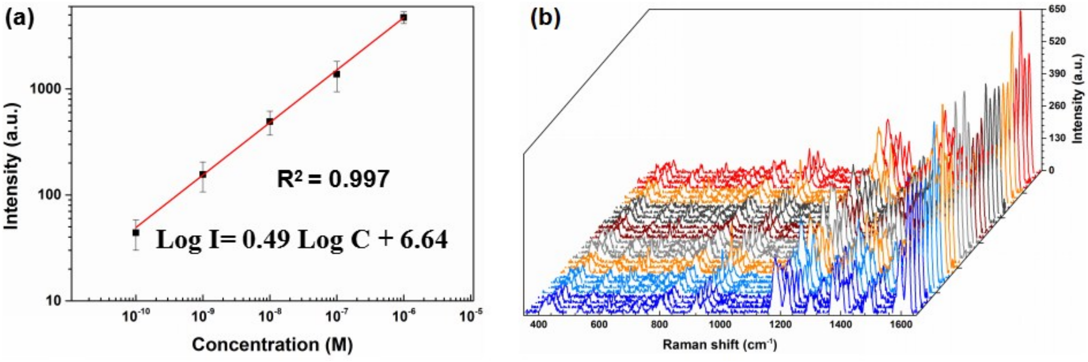

Fig. S9 (a) The calibration curve of normalized Raman intensity at 1179 cm^{-1} versus the concentration of MG. (b) 30 SERS spectra of MG (10^{-9} M) collected randomly from the 3D nanostructure.